

A low dissipation essentially non-oscillatory central scheme

R. Kissmann^{a,*}, R. Grauer^b,

^a *Institut für Theoretische Physik IV, Ruhr-Universität Bochum, 44780 Bochum, Germany*

^b *Institut für Theoretische Physik I, Ruhr-Universität Bochum, 44780 Bochum, Germany*

Abstract

Here we present a new, semidiscrete, central scheme for the numerical solution of one-dimensional systems of hyperbolic conservation laws. The method presented in this paper is an extension of the centrally weighted non-oscillatory schemes (CWENO) presented in [7], [5] and [6]. The method suggested in this manuscript is derived independently of the order of the scheme. The gain in this new method is a decreased dissipation especially for high Mach-number flows, which are frequently encountered, e. g., in astrophysical contexts or turbulent systems.

Key words: hyperbolic conservation laws, high resolution central schemes

1 Introduction

There are many methods available for the numerical solution of hyperbolic differential equations of the form:

$$\frac{\partial}{\partial t}u(x, t) + \frac{\partial}{\partial x}f(u(x, t)) = 0 \quad (1)$$

where $u(x, t)$ is a conserved quantity and $f(u(x, t))$ is a convection flux, which in most cases is nonlinear.

* Corresponding author.

Email addresses: rk@tp4.rub.de (R. Kissmann), grauer@tp1.rub.de (R. Grauer).

Of all the schemes available for the solution of such an equation the central schemes offer the advantage of simplicity as compared for example to upwind schemes (see e. g. in [12] or [4]). The first central scheme – the well-known Lax-Friedrichs scheme (see [3]), however, readily shows the most prominent problem of central schemes: they suffer from high numerical dissipation as compared to other (more complex) schemes. This issue was attacked by increasing the order of the scheme (see [9] for the first second order extension of the scheme and [8] for a third order version of the scheme) yielding a Centrally Weighted Non-Oscillatory Scheme (CWENO) of high order. Dissipation for small time-steps was reduced by the introduction of the semidiscrete version of these schemes (see [7] for the semidiscrete version of the second order scheme and [5] for the third order semidiscrete scheme) For high Mach-number flows, however, the dissipation becomes more and more dominant, due to the estimate for the Riemann fans getting worse. This could markedly be improved with a better estimate for the Riemann-fans (see [6]). Even then, however, the width of the Riemann fans still scales directly with the Mach number for high Mach number flows, thus, yielding poor results for the latter. Therefore, we followed the path taken by [6] even further, arriving at a scheme with significantly reduced dissipation where the Riemann fans do not depend on the Mach number of the flow. Especially for high Mach-number flows this scheme, described in this manuscript, delivers very encouraging results as is demonstrated with some examples. This feature is valuable for many applications of numerical schemes to e. g. high Mach-number astrophysical flows, which are known to frequently exceed Mach-numbers of five (see e. g. [1] or [13]).

2 The classical Cweno scheme

Before introducing the ideas of the new scheme we will briefly describe the CWENO scheme as presented in former publications. For a more detailed introduction see [7], [5] and references therein.

The basic idea for the classical central schemes is an integration of Eq. (1) over one small cell of width Δx and a small time-step Δt . Such an integration leads to an evolution equation for the *cell average* of the quantity $u(x, t)$. This equation usually gives the cell average at the new time-step against the cell average at the previous time-step and the fluxes at the cell boundaries. To obtain the quantities at the cell boundaries one also needs a piecewise polynomial reconstruction, which regains point-values from the cell averages – yielding different functions for each individual cell. For a first-order piecewise linear reconstruction one obtains the Lax-Friedrichs scheme given on a staggered grid.

Due to the different reconstructions in each cell one formally has a disconti-

nuity at each cell boundary. To avoid having to compute the exact solution of the corresponding Riemann-problems one, therefore, introduces the above integration over the whole region containing this Riemann fan.

While the integration for this averaging in the Lax-Friedrichs scheme is performed from cell centre to cell centre, in the CWENO scheme the averaging over the Riemann fan is done over a much smaller region. To achieve this, Eq. (1) is integrated over the volume containing the Riemann fans and over the *undisturbed* volume separately. By this, the dissipation can be significantly diminished, since only for the region containing the Riemann fan an averaging is applied, whereas the result for the undisturbed part of the cell is exact. Instead of an evolution equation for the cell average of the entire cell the integration over these sub-volumes and one time-step yields an evolution equation for the cell averages of the sub-volumes. By a projection of these *local* cell averages at the next time-step onto the original grid and the transition $\Delta t \rightarrow 0$ one finally arrives at a semidiscrete evolution scheme for the cell averages, which does not require a staggered grid anymore. The semidiscrete scheme is simply the approximation of the fully discrete scheme in the limit $\Delta t \rightarrow 0$ by:

$$\frac{d}{dt}u_i(t) = \lim_{\Delta t \rightarrow 0} \frac{u_i^n - u_{i-1}^n}{\Delta t} \quad (2)$$

The semidiscrete version of a CWENO scheme does not suffer from the accumulation of excessive dissipation for small time-steps as a fully discrete scheme would do. The time-step size of the latter are smaller due to a restricted CFL-condition $\Delta t \propto (\Delta x)^2$ – as opposed to the convective CFL-condition used in semidiscrete schemes. This small time-step size leads to an accumulation of the numerical dissipation as is argued in [7].

Concluding we remark, that the essential ingredient of the CWENO scheme, which leads to a major improvement over the staggered grid schemes like e. g. the Lax-Friedrichs, is the reduction of the averaging region containing the Riemann fan. It will, however, be discussed in the next section that the width of this region in the previous CWENO schemes is hugely overestimated for high Mach number flows. The scheme introduced in this article shows how to eliminate this shortcoming, giving a new scheme with minimised averaging regions based on the previous CWENO scheme.

3 The new scheme

The CWENO scheme described briefly in the preceding section is robust, essentially non-oscillatory, one whose main feature is its simplicity. In consecutive publications its inventors suggested less and less dissipative schemes. Part of

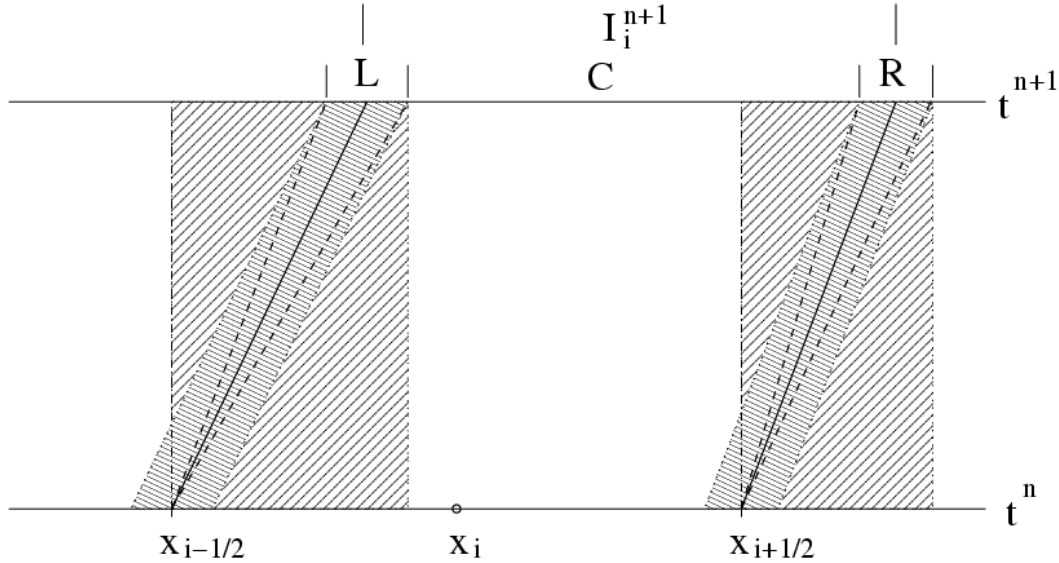


Fig. 1. Typical Riemann fan structure for high Mach number flow.

this goal was achieved by increasing the order of the piecewise reconstruction of point values from the cell averages (see, e. g. [5] for the step from second to third order).

A major part of the dissipation inherent in the CWENO scheme is, however, connected to the width of the regions assumed to contain the Riemann fans. The dissipation was markedly reduced again, when the estimate for the extent of the Riemann fans was refined in [6]. In this publication the authors distinguished the possible propagation speed of the Riemann fans to the left and to the right. If, e. g., the velocity of a fluid to be computed exactly equals the maximum propagation speed of any signal in the fluid a shock can not propagate upstream, and the region over which the averaging for the Riemann fans is applied extends only into one cell. In the case, where the distinction of the propagation direction is not made the averaging region extends symmetrically into both cells under consideration. Thus, this region is twice as wide as for the refined scheme.

If the scheme is, however, applied to high Mach number flows, the flow velocity on average exceeds the maximum propagation speed of signals in the fluid. Then the width of the regions over which the integration takes place is roughly given by the speed of the flow times the time-step (or rather twice that value if the directional distinction is not made). The actual width of the region where the shock can possibly be is, however, only two times the maximum signal propagation speed times the time-step. Since this differs markedly from the assumption in the CWENO scheme, we felt that it might be interesting to pursue the approach from [6] a little further in search of a scheme with even less dissipation.

To motivate our new approach one can imagine a typical flow structure of a conservative system of equations as given in Fig. 1. What is depicted there is the case for a supersonic flow directed to the right. The cell under consideration with centre at x_i has boundaries at $x_{i-1/2}$ and $x_{i+1/2}$. The two horizontal lines indicate two successive time-steps. The average flow velocity at the boundary of the cell at the first of these time-steps is indicated by the solid line as the position taken by a particle convected with that velocity. In the same way the maximum propagation speed of signals are indicated as the dashed lines – clearly we are discussing supersonic flow.

The region in which the averaging over the Riemann fans is carried out in the Kurganov et al.- version (see [6]) of the scheme is indicated as the filled rectangle on each boundary of the cell. The position of a possible discontinuity, which gives rise to the idea of the averaging, however, can only be found between the dashed lines. Therefore, we suggest an alternative derivation of the CWENO scheme, where the domains over which the integration takes place are not rectangular any more.

Here we perform the averaging instead over the shaded parallelogram regions indicated in Fig. 1. The main difference is, that the position of the boundaries for the integral over the spatial domains now depend on time. The width of the Riemann fans, however, is given only by the maximum signal propagation velocity so that the background flow does not change the width of the fans – in contrast to the other schemes.

For these regions one can derive a scheme very similar to the others when using exactly the same steps as were used for the established CWENO scheme: first we integrate the regions of smooth flow and the regions which might hold discontinuities separately. Then we obtain a new reconstruction for these regions and finally project all this back onto the desired spatial grid. The first step in this scheme is the integration of the different regions. This is done in the following section for the smooth and discontinuous regions separately.

3.1 Integration of the discontinuities

Since the averaging is to take place over a region inclined with the local average velocity we have to deal with smaller Riemann-fans than they are used in the established CWENO scheme for high Mach-number flows. Here the width of the Riemann fans is basically given by twice the maximum signal propagation velocity (possibly running to the left or to the right) – behold that this signal propagation is only possible relative to the average fluid velocity). In subsequent computations we will use the following conventions for the different

velocities:

$$\begin{aligned} v_{i-1/2}^0 &\rightarrow \text{local average velocity} \\ a_{i-1/2}^\pm &\rightarrow \text{right (left) maximum signal velocity relative to } \textit{local} \text{ mean flow} \end{aligned} \quad (3)$$

As mentioned already, the solution can only be discontinuous in the hatched parallelogram regions. Assuming the velocities are constant for a small time dt time the region is given by:

$$\begin{aligned} [x_{i-1/2,l}^n, x_{i-1/2,r}^n] = \\ [x_{i-1/2} - a_{i-1/2}^- \Delta t + v_{i-1/2}^0(t - t^n), x_{i-1/2} + a_{i-1/2}^+ \Delta t + v_{i-1/2}^0(t - t^n)] \end{aligned} \quad (4)$$

So we see that the region is shifted to the right with the corresponding average velocity. For the integration over this particular region and the time interval $[t^n, t^{n+1}]$ one has to keep in mind, that we have to do the spatial integration first due to the dependence of its boundaries on time. Integration of Eq. (1) over space and time then yields:

$$\int_{t^n}^{t^{n+1}} \left(\int_{x_{i-1/2,l}(t)}^{x_{i-1/2,r}(t)} \frac{\partial}{\partial t} u \, dx \right) dt = - \int_{t^n}^{t^{n+1}} \left(\int_{x_{i-1/2,l}(t)}^{x_{i-1/2,r}(t)} \frac{\partial f}{\partial x} dx \right) dt \quad (5)$$

To evaluate the left-hand side of this equation we have to use:

$$\frac{d}{dt} \int_{a(t)}^{b(t)} g(x, t) dx = \frac{db}{dt} g(b, t) - \frac{da}{dt} g(a, t) + \int_{a(t)}^{b(t)} \frac{\partial}{\partial t} g(x, t) dx \quad (6)$$

For our case this translates into:

$$\begin{aligned} &\int_{t^n}^{t^{n+1}} \left(\int_{x_{i-1/2,l}(t)}^{x_{i-1/2,r}(t)} \frac{\partial}{\partial t} u \, dx \right) dt \\ &= \int_{t^n}^{t^{n+1}} \left(\frac{d}{dt} \int_{x_{i-1/2,l}(t)}^{x_{i-1/2,r}(t)} u(x, t) \, dx \right) dt \\ &\quad - \int_{t^n}^{t^{n+1}} \left(u(x_{i-1/2,r}, t) \frac{d}{dt} x_{i-1/2,r} - u(x_{i-1/2,l}, t) \frac{d}{dt} x_{i-1/2,l} \right) dt \end{aligned}$$

$$\begin{aligned}
&= \int_{x_{i-1/2,l}(t^{n+1})}^{x_{i-1/2,r}(t^{n+1})} u(x, t^{n+1}) dx - \int_{x_{i-1/2,l}(t^n)}^{x_{i-1/2,r}(t^n)} u(x, t^n) \\
&\quad - \int_{t^n}^{t^{n+1}} \left(v_{i-1/2}^0 \left[u(x_{i-1/2,r}, t) - u(x_{i-1/2,l}, t) \right] \right) dt
\end{aligned} \tag{7}$$

due to the dependence of the domains on time. Here the terms containing $v_{i-1/2}^0$ are introduced due to the time dependence of the cell boundary positions. Then we find using Eqs. (7) and (5) (and designating the average for this region at time t^{n+1} as $\bar{\omega}_{i-1/2}^{n+1}$):

$$\begin{aligned}
&\int_{t^n}^{t^{n+1}} \left(\int_{x_{i-1/2,l}(t)}^{x_{i-1/2,r}(t)} \frac{\partial}{\partial t} u dx \right) dt \\
&= (x_{i-1/2,r}(t^{n+1}) - x_{i-1/2,l}(t^{n+1})) \bar{\omega}_{i-1/2}^{n+1} - \int_{x_{i-1/2,l}(t^n)}^{x_{i-1/2,r}(t^n)} u dx \\
&\quad - \int_{t^n}^{t^{n+1}} \left(v_{i-1/2}^0 \left[u(x_{i-1/2,r}(t)) - u(x_{i-1/2,l}(t)) \right] \right) \\
&= - \int_{t^n}^{t^{n+1}} \left(\int_{x_{i-1/2,l}(t)}^{x_{i-1/2,r}(t)} \frac{\partial f}{\partial x} dx \right) dt
\end{aligned} \tag{8}$$

Here the boundaries of the region are given by:

$$\begin{aligned}
x_{i-1/2,l}(t) &= x_{i-1/2} - a_{i-1/2}^- \Delta t + v_{i-1/2}^0 (t - t^n) \\
x_{i-1/2,r}(t) &= x_{i-1/2} + a_{i-1/2}^+ \Delta t + v_{i-1/2}^0 (t - t^n)
\end{aligned} \tag{9}$$

as was given in Eq. (4) With this in mind we also perform the flux integration, thus arriving at an intermediate result for the local average at the next time-step t^{n+1} :

$$\begin{aligned}
\bar{\omega}_{i-1/2}^{n+1} &= \frac{1}{x_{i-1/2,r}(t^{n+1}) - x_{i-1/2,l}(t^{n+1})} \left(\int_{x_{i-1/2,l}(t^n)}^{x_{i-1/2,r}(t^n)} u dx \right. \\
&\quad \left. + \int_{t^n}^{t^{n+1}} \left(v_{i-1/2}^0 \left(u(x_{i-1/2,r}(t)) - u(x_{i-1/2,l}(t)) \right) \right) dt \right)
\end{aligned}$$

$$\begin{aligned}
& - \int_{t^n}^{t^{n+1}} \left(f(u(x_{i-1/2,r}, t)) - f(u(x_{i-1/2,l}, t)) \right) dt \\
= & \frac{1}{x_{i-1/2,r}(t^{n+1}) - x_{i-1/2,l}(t^{n+1})} \left(\int_{x_{i-1/2,l}(t^n)}^{x_{i-1/2}} p_{i-1}^n dx + \int_{x_{i-1/2}}^{x_{i-1/2,r}(t^n)} p_i^n dx \right. \\
& - \int_{t^n}^{t^{n+1}} \left(f(u(x_{i-1/2,r}, t)) - v_{i-1/2}^0 u(x_{i-1/2,r}(t)) \right) dt \\
& \left. + \int_{t^n}^{t^{n+1}} \left(f(u(x_{i-1/2,l}, t)) - v_{i-1/2}^0 u(x_{i-1/2,l}(t)) \right) dt \right) \quad (10)
\end{aligned}$$

Here we introduced the representation of the quantity u by a polynomial p_i^n given for each individual cell. For the region under consideration we have to deal with two different polynomials, since we are considering a domain extending into two neighbouring cells.

Apart from the additional flux-terms $v_{i-1/2}^0 u(x_{i-1/2,i}(t))$ this result looks familiar when consulting the previous publications (see e. g. [6]). The interpretation, however, is quite different: on the one hand the cell average $\bar{\omega}_{i-1/2}^{n+1}$ is not given at the same location as $\bar{\omega}_{i-1/2}^n$. On the other hand one has to evaluate the flux integral for time-dependent boundaries.

Keeping this in mind the integral for the central part of the cell can be computed in the same way resulting in the expression:

$$\begin{aligned}
\bar{\omega}_i^{n+1} = & \frac{1}{x_{i+1/2,l}(t^{n+1}) - x_{i-1/2,r}(t^{n+1})} \left(\int_{x_{i-1/2,r}(t^n)}^{x_{i+1/2,l}(t^n)} p_i^n dx + \right. \\
& - \int_{t^n}^{t^{n+1}} \left(f(u(x_{i+1/2,l}, t)) - v_{i+1/2}^0 u(x_{i+1/2,l}(t)) \right) dt \\
& \left. + \int_{t^n}^{t^{n+1}} \left(f(u(x_{i-1/2,r}, t)) - v_{i-1/2}^0 u(x_{i-1/2,r}(t)) \right) dt \right) \quad (11)
\end{aligned}$$

We note the following:

- Considering the above equation for an exclusive transport case motivates the validity of the formula. If for example only the velocities at the upper and lower cell boundary differ, with the flux in the cell being constant, then the dominant effect is the increase or decrease of the cell average $\bar{\omega}$ due to the different size of the cell at times t^n and t^{n+1} .
- The velocity suggested to be chosen for $v_{i\pm 1/2}^0$ is the local average velocity

as was mentioned above. It is, however, also possible to use a more global choice. For example for a global background flow velocity would also be an appropriate choice for this. This would then keep the cell sizes constant and yield a less dissipative scheme at the same time.

- Remember that $a_{i-1/2}^{\pm}$ designates the local maximum signal propagation velocity relative to the local background flow velocity $v_{i-1/2}^0$.
- In the limit of high Mach numbers the velocities $a_{i-1/2}^{\pm}$ can be directly given as the maximum signal propagation velocity. Otherwise there usually is a different local velocity obtained from the reconstruction in adjacent cells. This has to be taken into account, by adding the maximum difference from the average velocity to the maximum signal propagation velocity.

The next step in the classic CWENO scheme would be the projection back onto the original grid, where the conservation property of the reconstruction for the central part of the cell is used when obtaining new cell averages. With the inclined averaging regions for the Riemann-fans, however, this means that we have to project onto shifted cells, with the shift of their corresponding boundaries given by the local velocities $v_{i\pm 1/2}^0$.

Then again it would also be possible to project the local averages back onto the original unshifted grid. This would, however, be more involved due to the shift of the cells and due to the fact, that the conservation property for the central part of the cell can not be used anymore in most cases – for example the conservation property of the reconstruction for the central part of the cell is of no use whenever this region has to be projected onto more than one of the cells (i. e. whenever $v_{i+1/2}^0 > a_{i+1/2}^-$ or $v_{i-1/2}^0 < -a_{i-1/2}^+$). To retain the simplicity of the CWENO scheme we will here omit the discussion of such a projection onto the original grid.

First we project the values not onto the actual grid, but onto the *transported* grid, thus, obtaining cell averages for a not necessarily homogeneous grid. The cell averages can then be projected back onto the original grid whenever necessary. For this one would use an additional reconstruction step, where the full order of the reconstruction has to be used to keep the desired order of the scheme.

The width and position of the grid cells at the next time-step becomes clear from Fig. 1 and from Eq. (4). With the *local* transport velocity v^0 this reads:

$$I_i^{n+1} = [x_{i+1/2}^{n+1} - x_{i-1/2}^{n+1}] = [(x_{i+1/2}^n + v_{i+1/2}^0 \Delta t) - (x_{i-1/2}^n + v_{i-1/2}^0 \Delta t)] \quad (12)$$

To be able to project the local cell averages onto this grid we use a polynomial reconstruction for time-step t^{n+1} : we construct a new non-oscillatory global

piecewise interpolant from the local cell averages at time t^{n+1} as:

$$\tilde{\omega}^{n+1}(x) = \sum_i \left(\tilde{\omega}_{i-1/2}^{n+1}(x) \chi_{[x_{i-1/2,l}^{n+1}, \dots, x_{i-1/2,r}^{n+1}]} + \tilde{\omega}_i^{n+1}(x) \chi_{[x_{i-1/2,r}^{n+1}, \dots, x_{i+1/2,l}^{n+1}]} \right) \quad (13)$$

From this we obtain the cell averages on the shifted grid by:

$$\bar{u}_i^{n+1} = \frac{1}{\tilde{\Delta}x} \int_{x_{i-1/2}^{n+1}}^{x_{i+1/2}^{n+1}} \tilde{\omega}^{n+1}(x) dx \quad (14)$$

where $\tilde{\Delta}x$ is the width of the shifted cell I_i^{n+1} . Since we are interested in the semidiscrete version of the scheme we proceed by expressing the time derivative by:

$$\frac{d}{dt} \bar{u}_i(t) = \lim_{\Delta t \rightarrow 0} \frac{\bar{u}_i^{n+1} - \bar{u}_i^n}{\Delta t} = \lim_{\Delta t \rightarrow 0} \left(\frac{1}{\tilde{\Delta}x} \int_{x_{i-1/2}^{n+1}}^{x_{i+1/2}^{n+1}} \tilde{\omega}^{n+1}(x) dx - \bar{u}_i^n \right) \quad (15)$$

where one has to keep in mind, that u^{n+1} is given at another position on the spatial grid than u^n .

For this we need to evaluate the integrals over the smooth and non-smooth parts of the shifted cells. Due to the conservation property of the reconstruction for the smooth part of the cell (in the shifted frame) we have:

$$\frac{1}{x_{i+1/2,l}(t^{n+1}) - x_{i-1/2,r}(t^{n+1})} \int_{x_{i-1/2,r}(t^{n+1})}^{x_{i+1/2,l}(t^{n+1})} \tilde{\omega}_i^{n+1}(x) dx = \bar{u}_i^{n+1}(x) \quad (16)$$

Apart from that for the non-smooth parts of the cell the limited width of the Riemann-fans in the limit $dt \rightarrow 0$ leads to the result:

$$\tilde{\omega}_{i\pm 1/2}^{n+1}(x) = \bar{\omega}_{i\pm 1/2}^{n+1}(x) + \mathcal{O}(\Delta t) \quad (17)$$

Thus, we find in the semidiscrete limit ($dt \rightarrow 0$):

$$\begin{aligned} \frac{d}{dt} \bar{u}_i(t) = \lim_{\Delta t \rightarrow 0} \frac{1}{\Delta t} & \left(\frac{L_i \cap I_i^{n+1}}{\tilde{\Delta}x} \bar{\omega}_{i-1/2}^{n+1} + \frac{C_i^{n+1}}{\tilde{\Delta}x} \bar{\omega}_i^{n+1} \right. \\ & \left. + \frac{R_i \cap I_i^{n+1}}{\tilde{\Delta}x} \bar{\omega}_{i+1/2}^{n+1} - \bar{u}_i^n \right) \end{aligned} \quad (18)$$

where I^{n+1} indicates the shifted cell at t^{n+1} . The individual domains needed here are given in the semidiscrete limit as:

$$L_i \cap I_i^{n+1} = x_{i-1/2,r}(t^{n+1}) - x_{i-1/2}(t^{n+1}) = a_{i-1/2}^+ \quad (19)$$

$$C_i^{n+1} = x_{i+1/2,l}(t^{n+1}) - x_{i-1/2,r}(t^{n+1}) \quad (20)$$

$$R_i \cap I_i^{n+1} = x_{i+1/2}(t^{n+1}) - x_{i+1/2,l}(t^{n+1}) = a_{i+1/2}^- \quad (21)$$

What is still missing are the cell averages for the smooth and non-smooth regions. Beginning with the latter of those (here we have to keep in mind that we have $R_{i-1} = L_i$) we find by usage of Eq. (10):

$$\begin{aligned} \lim_{\Delta t \rightarrow 0} \bar{\omega}_{i-1/2}^{n+1} &= \frac{a_{i-1/2}^- u_{i-1/2}^- + a_{i-1/2}^+ u_{i-1/2}^+}{(a_{i-1/2}^+ + a_{i-1/2}^-)} - \frac{(f(u_{i-1/2}^+) - v_{i-1/2}^0 u_{i-1/2}^+)}{(a_{i-1/2}^+ + a_{i-1/2}^-)} \\ &\quad + \frac{(f(u_{i-1/2}^-) - v_{i-1/2}^0 u_{i-1/2}^-)}{(a_{i-1/2}^+ + a_{i-1/2}^-)} \quad (22) \end{aligned}$$

The computation for the central part is a little more involved and can be shown to yield:

$$\begin{aligned} \lim_{\Delta t \rightarrow 0} \bar{\omega}_i^{n+1} &= \frac{\bar{u}_i^n \Delta x - (a_{i-1/2}^+ u_{i-1/2}^+ + a_{i+1/2}^- u_{i+1/2}^-) \Delta t}{(x_{i+1/2,l}(t^{n+1}) - x_{i-1/2,r}(t^{n+1}))} \\ &\quad - \frac{(f(u_{i+1/2}^-) - v_{i+1/2}^0 u_{i+1/2}^-)}{(x_{i+1/2,l}(t^{n+1}) - x_{i-1/2,r}(t^{n+1}))} \Delta t \\ &\quad + \frac{(f(u_{i-1/2}^+) - v_{i-1/2}^0 u_{i-1/2}^+)}{(x_{i+1/2,l}(t^{n+1}) - x_{i-1/2,r}(t^{n+1}))} \Delta t \quad (23) \end{aligned}$$

Both of these can be recast into:

$$\lim_{\Delta t \rightarrow 0} \bar{\omega}_{i-1/2}^{n+1} = \frac{\tilde{a}_{i-1/2}^- u_{i-1/2}^- + \tilde{a}_{i-1/2}^+ u_{i-1/2}^+}{(a_{i-1/2}^+ + a_{i-1/2}^-)} - \frac{(f(u_{i-1/2}^+) - f(u_{i-1/2}^-))}{(a_{i-1/2}^+ + a_{i-1/2}^-)} \quad (24)$$

$$\begin{aligned} \lim_{\Delta t \rightarrow 0} \bar{\omega}_i^{n+1} &= \frac{\bar{u}_i^n \Delta x - (\tilde{a}_{i-1/2}^+ u_{i-1/2}^+ + \tilde{a}_{i+1/2}^- u_{i+1/2}^-) \Delta t}{(x_{i+1/2,l}(t^{n+1}) - x_{i-1/2,r}(t^{n+1}))} \\ &\quad - \frac{(f(u_{i+1/2}^-) - f(u_{i-1/2}^+))}{(x_{i+1/2,l}(t^{n+1}) - x_{i-1/2,r}(t^{n+1}))} \Delta t \quad (25) \end{aligned}$$

where we introduced the velocities:

$$\tilde{a}^+ = a^+ + v^0 \quad \text{and} \quad \tilde{a}^- = a^- - v^0 \quad (26)$$

for each of the positions in the numerical scheme. These are essentially the absolute maximum signal propagation velocities – that is these are given in the absolute frame and not relative to a possible background flow.

Consequently, we find:

$$\begin{aligned} \lim_{\Delta t \rightarrow 0} \frac{1}{\Delta t} \left(\frac{C_i^{n+1}}{\tilde{\Delta x}} \bar{w}_i^{n+1} - \bar{u}_i^n \right) &= - \frac{\tilde{a}_{i-1/2}^+ u_{i-1/2}^+ + \tilde{a}_{i+1/2}^- u_{i+1/2}^-}{\tilde{\Delta x}} \\ &- \frac{(f(u_{i+1/2}^-) - f(u_{i-1/2}^+))}{\tilde{\Delta x}} + \frac{1}{\Delta t} \left(\frac{\Delta x}{\tilde{\Delta x}} - 1 \right) \bar{u}_i^n \end{aligned} \quad (27)$$

and:

$$\frac{1}{\Delta t} \left(\frac{\Delta x}{\tilde{\Delta x}} - 1 \right) \bar{u}_i^n = (v_{i+1/2}^0 - v_{i-1/2}^0) \bar{u}_i^n \quad (28)$$

Inserting this, together with the results for the other terms obtained above, into Eq. (18) yields:

$$\frac{d}{dt} \bar{u}_i(t) = - \frac{H_{i+1/2} - H_{i-1/2}}{\tilde{\Delta x}} + (v_{i+1/2}^0 - v_{i-1/2}^0) \bar{u}_i^n \quad (29)$$

where we introduced:

$$\begin{aligned} H_{i+1/2} &= - \frac{\tilde{a}_{i+1/2}^+ a_{i+1/2}^- u_{i+1/2}^+ - a_{i+1/2}^+ \tilde{a}_{i+1/2}^- u_{i+1/2}^-}{a_{i+1/2}^+ + a_{i+1/2}^-} \\ &+ \frac{a_{i+1/2}^+ f(u_{i+1/2}^-) + a_{i+1/2}^- f(u_{i+1/2}^+)}{a_{i+1/2}^+ + a_{i+1/2}^-} \end{aligned} \quad (30)$$

Obviously we found a result very similar to that for the classical CWENO scheme. The main differences are that we have to distinguish between the two different kinds of velocities and that the resulting changes are given for the shifted grid. Also the correction term $(v_{i+1/2}^0 - v_{i-1/2}^0) \bar{u}_i^n$ has to be included. This term ensures change of the cell average, whenever the cell size is modified.

We note:

- The resulting evolution requires a moving, generally non-uniform grid. The cell averages at the next time-step are in general given at a shifted position. This shift depends on the velocity v^0 at the individual cell boundaries. This usually poses no problems (for limits on this see section 5). The main limitation in a one-dimensional computation is that one has to take the varying sizes of the individual cells into account, when computing the reconstruction for the next time-step. Whenever an output on an equidistant grid is

desired or the individual cells get too big or too small the results can be projected back to the original grid.

- The shift of each individual cell is given by:

$$\delta x_{i-1/2} = \int_{t^0}^t v_{i-1/2}^0(t) dt \quad (31)$$

for the lower boundary of cell I_i . From this the actual size of the corresponding cell is easily computed.

- Alternatively the projection back onto the equidistant grid can be performed after each successfully completed time-step. Such a scheme would, however, become more complicated.
- The velocity v^0 at the boundary of the individual cell does not have to be the local average - one could also use a global average instead. This does not change the above results at all.
- The CFL condition for the above scheme to remain mathematically sensible is obtained by the fact, that the regions containing the Riemann fans must not intersect. This is ensured by:

$$\Delta t < \frac{\Delta x}{2} \frac{1}{\max(a^\pm)} \quad (32)$$

whereas the previous CWENO schemes had to use $\max(a^\pm + v^0)$ instead of $\max(a^\pm)$. This advantage is, however, put into perspective, when taking into account, that the varying size of the grid cells in the new scheme effects a smaller Δx for some cells as compared to the unmodified grid.

This concludes the derivation and description of the scheme. To motivate the usefulness of the scheme we will now discuss a few illustrative test-cases.

4 Test problems

Since the scheme developed in this manuscript is a strict one dimensional scheme, we only discuss a few one dimensional tests. Despite the fact that *linear* transport is solved exactly by this scheme we will nonetheless start our discussion by this to show its power. Please be aware that all of the following test problems are given in non-dimensional form.

4.1 Linear transport

For a strictly linear transport problem, which is quite often employed to determine the order of a numerical scheme the scheme presented in this manuscript

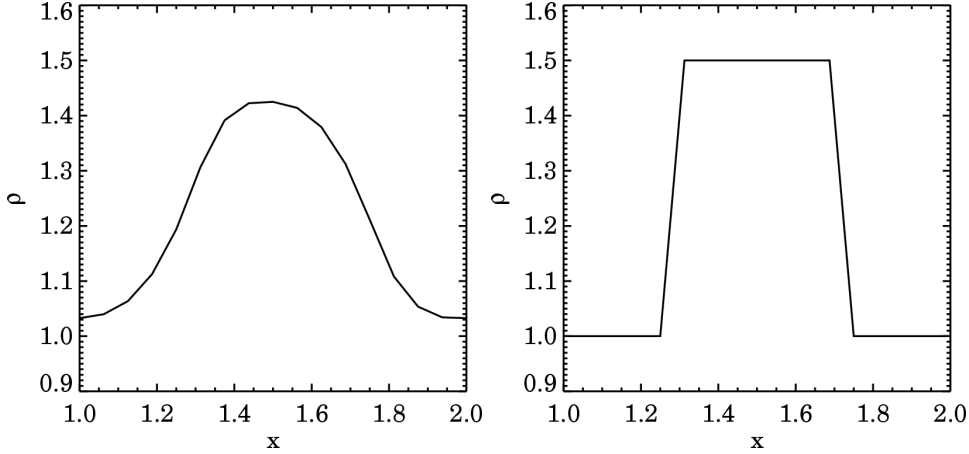


Fig. 2. Resulting density profiles for the linear transport problem of a box like density enhancement for the classical (left) and the new (right) CWENO scheme.

is naturally dissipation free. This is due to the fact that the flux for linear transport is equivalent to the global mass flux $\tilde{v}u$ in Eq. (30). Therefore, all the terms cancel for all individual cells, thus, leaving all cell averages unchanged. The only change resulting in linear transport is the transport of the cell boundaries all with the same velocity. This means that the initial profile is just transported along with the desired velocity as is to be expected in linear transport. The initial conditions corresponding to this problem simply read:

$$\rho(x) = \begin{cases} 1.5 & \text{if } x \geq 0.25 \cap x \leq 0.75 \\ 1 & \text{else} \end{cases} \quad (33)$$

with a constant velocity $v = 1$.

In Fig. 2 the result of such a computation is compared to the result obtained using the classical CWENO scheme. Here an initial box-like density enhancement was transported from $x = 0.5$ to $x = 1.5$ with a velocity of $v = 1$. The results in Fig. 2 are shown at a time $t = 1$. For both simulations we chose the time-step to be 0.01 which yields a CFL-number (being defined as the ratio of the distance travelled by a signal in one time-step to the size of a grid cell) of 0.16 for a decomposition of the computational domain into 16 cells. Clearly there is no dissipation when using the new method as can be expected from the scheme.

The next test was a little more involved. As a result it showed the strength and at the same time the weakness of the scheme, leading to the conclusion, that the scheme is especially suited for high Mach number flows.

4.2 Strong shock tube

The second test is a modification of the shock tube problem first used by Sod [10]. Here we used the strong shock tube problem (see [2]) with the initial condition:

$$[\rho(x), p(x)] = \begin{cases} [10, 100] & \text{if } x < 0.5 \\ [1, 1] & \text{if } x \geq 0.5 \end{cases} \quad (34)$$

In this test the resulting gradients are even stronger than in the classical shock tube problem. The above was used as the initial condition for the 1-D Euler system:

$$\frac{\partial}{\partial t} \rho = -\frac{\partial}{\partial x} s \quad (35)$$

$$\frac{\partial}{\partial t} s = -\frac{\partial}{\partial x} (s^2/\rho + p) \quad (36)$$

$$\frac{\partial}{\partial t} e = -\frac{\partial}{\partial x} ((e + p) s/\rho) \quad (37)$$

where ρ is the mass density, s is the mass flux $s = \rho u$ and e is the total energy density. In one of our simulation this system was subjected to a high Mach number initial background flow to directly visualise the problems inherent in the classical scheme concerning high Mach number flows. For this we chose a flow velocity of $v_0 = 20$. With the initial configuration yielding a speed of sound of $c_s = 3.74$ to the left of the contact discontinuity and $c_s = 1.18$ to the right, this choice for the flow velocity corresponds to Mach numbers of 5.3 and 16.9 respectively. Clearly, this kind of background flow can be eliminated by a Galilei-transformation. This however is not possible in the general case. With the need to compare the results to an analytical solution, however, we needed to use a constant background flow.

The system was solved for $0 \leq x \leq 1$ at $t = 0$ and integrated up to $t = 0.08$. Here the time evolution is carried out using the third order explicit Runge-Kutta method, where the time-step was chosen as $5 \cdot 10^{-5}$ as to give a CFL number < 0.2 at all times. Initially we used a size of $5 \cdot 10^{-3}$ for each grid cell, which is modified when using the new scheme.

At time $t = 0.08$ a strong rarefaction wave, a contact discontinuity and a strong shock (from left to right in figures 3 and 4 respectively) have developed. In both figures we show a comparison of the solutions obtained with and without the background flow to the analytical solution.

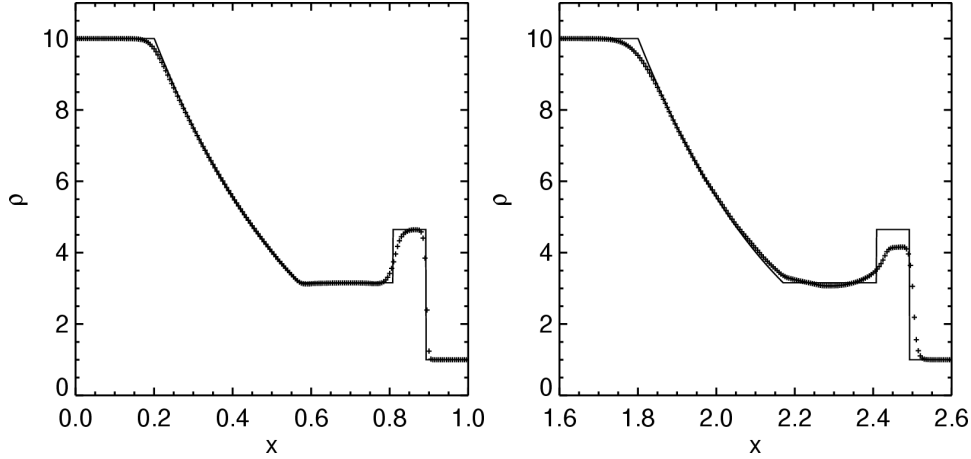


Fig. 3. Resulting density distribution for the strong shock tube problem at time $t = 0.08$ using the classical CWENO scheme. Here we compare the solution with (left) and without (right) background flow to the analytical solution (solid line).

The results shown in Fig 3 were obtained using the classical CWENO scheme with a second order reconstruction. The solution without background flow (left) shows the ability of the scheme to nicely reproduce discontinuities. The solution on the right, however, clearly shows the dependence of the solution on the speed of the background flow. Obviously the solution in the right part of the domain is poorly resolved: the density in the region between the contact discontinuity and the shock never gets near the analytical value anymore.

The reason for the solution on the left hand side of the contact discontinuity to be better than on the right hand side is given by the arguments in the introductory discussion: the Mach number for the background flow is higher on the right side of the discontinuity than on the left, which is due to the higher sound speed on the left as compared to the right side: in the unperturbed regions the Mach number clearly sticks to the initial value. In the vicinity of the discontinuity, however, the Mach number rises due to the rising pressure to a value between 5 and 8 in the region of the discontinuity and the rarefaction wave.

Keeping all this in mind Fig. 3 clearly confirms the weakness of the CWENO scheme in handling high Mach number flows.

For the new scheme we used the identical second order reconstruction as for the classical CWENO scheme. The corresponding results are finally illustrated in Fig. 4 in the same way as we gave the results for the old scheme. With the crosses indicating the position of the cell centres the propagation of the cells becomes clearly visible. In this computation we did never project the data back onto the original grid. This leads to the depletion of grid-points in the region left of the contact discontinuity. Due to this depletion the result for that region is inferior to the computation using the classical CWENO scheme, when

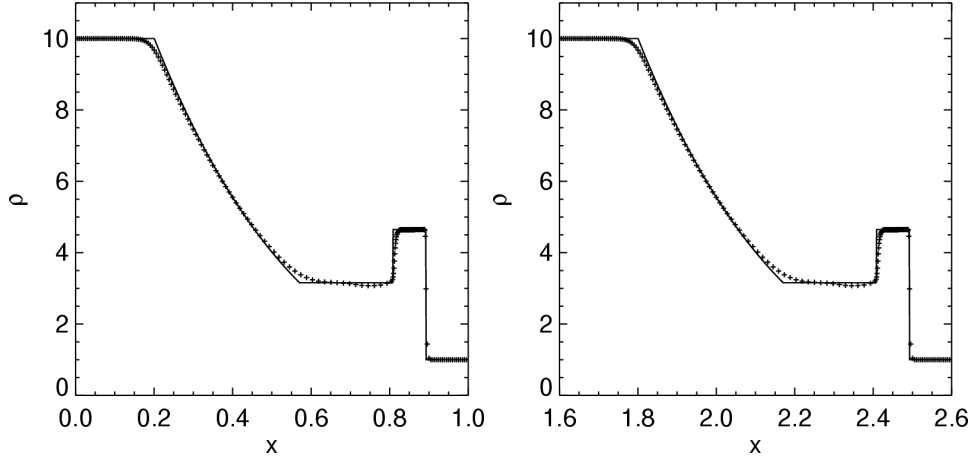


Fig. 4. Resulting density distribution for the strong shock tube problem at time $t = 0.08$ using the new CWENO scheme. Here we compare the solution with (left) and without (right) background flow to the analytical solution (solid line).

no background flow is present. In the region right of the contact discontinuity, however, the grid-points are *piled up* leading to superior results in that region. Here one has to keep in mind, that the velocity at the boundaries of the grid cells is not only given by the background velocity but by the sum of this and the local velocity – thus, there is also a redistribution of the cells when now background flow is present.

Yet the most important result visible in Fig. 4 is the expected fact, that the solution is completely independent of the background flow: the solution does not change at all, when a high Mach number background flow is present. Therefore, we were able to confirm that the numerical dissipation for this scheme is entirely independent of the Mach number of any background flow.

Above all, it is also evident, that the results for high Mach number flows are much better using the new scheme. Especially in the region to the right of the contact discontinuity the solution for the classical CWENO scheme becomes poor for high Mach number flows. The new scheme, however yields consistently very accurate solutions for this region.

5 Restrictions

For the above test cases the solutions were computed solely on the co-moving grid without ever projecting it back to the original grid. This was done to keep the scheme as simple as the classical CWENO scheme. As became apparent in the second test-case, however, gradients of the velocity cause a depletion of grid-points in some regions and an accumulation of grid-points in other regions. This leads to inferior results, where grid-points are depleted and in superior

results in regions with more grid-points.

A higher density of grid-points, however, also affects the CFL number, since this contains the inverse of the cell width. This effect is partly compensated by the fact, that the local average velocity is not included in the CFL number anymore.

Both these problems can be addressed by a modification of the scheme, where the computation is performed on the regular grid. In this case, however, the resulting scheme becomes more complex than the classical CWENO scheme. Therefore, this matter is not discussed in this paper any further and will be left for future publications.

One additional point to make is that due to the two problems mentioned above the scheme is not as easily applicable to all hyperbolic problems as was the classical CWENO scheme. When all the computations are realised on the co-moving grid, e. g. Burgers equation can not be adequately solved by the scheme. This is due to the fact, that all grid points are advected into the discontinuities and cover an infinitely small region. This, also, would pose no problem anymore for a scheme *living* only on a regular grid.

The computation on a regular grid is also a necessary ingredient for the extension of the scheme to more than one dimension. In this case the scheme can easily be extended e. g. using the dimension by dimension approach also used in [5]. This issue, however, is left for future publication.

6 Conclusion

Here we presented an improvement of the CWENO scheme, which proved very reliable in resolving discontinuities resulting from the solution of conservative systems of differential equations. The improvement is a more precise estimate of the width of the Riemann fans over which a spatial averaging is carried out in the derivation of the scheme. We were able to show how this leads to a scheme, which is in contrast to previous versions of the CWENO scheme entirely independent of any background flow. Therefore, the new scheme is especially suited for the computation of high Mach number flows as they are frequently encountered in astrophysical flows.

Furthermore we were able to show, that the scheme computes linear transport entirely free of numerical dissipation. Also the results for discontinuities in the flow for the solution of the Euler equation could be shown to be very accurate even in low Mach number simulations.

The scheme proposed in this paper enjoys the advantage of simplicity as the previous versions of the CWENO scheme: it is as easily implemented as was the classical CWENO scheme before. The overall structure of the equations to be integrated numerically differs only marginally from those of the classical scheme, but the differences are quite strong since the results have to be considered to be on a moving grid in the new scheme.

The new scheme, when computed exclusively on the co-moving grid, combines features of a fully Lagrangian scheme with the ideas of the classical CWENO scheme. Unfortunately, however, it is not as versatile as the classical CWENO scheme. To obtain an equally versatile scheme one has to switch over from the fully Lagrangian picture to a semi-Lagrangian picture (see e. g. [11]) i. e. the projection onto a non moving grid has to be added to the scheme. This, however, is left for future publications.

Acknowledgements

The authors would like to thank Dr. Horst Fichtner for valuable discussions on the manuscript.

This work was partially financed by the Deutsche Forschungsgemeinschaft (DFG) through the Sonderforschungsbereich SFB 591.

References

- [1] Boldyrev, S., Nordlund, Å., Padoan, P., Jul. 2002. Scaling Relations of Supersonic Turbulence in Star-forming Molecular Clouds. *ApJ*573, 678–684.
- [2] Calder, A. C., Fryxell, B., Plewa, T., Rosner, R., Dursi, L. J., Weirs, V. G., Dupont, T., Robey, H. F., Kane, J. O., Remington, B. A., Drake, R. P., Dimonte, G., Zingale, M., Timmes, F. X., Olson, K., Ricker, P., MacNeice, P., Tufo, H. M., Nov. 2002. On Validating an Astrophysical Simulation Code. *ApJS*143, 201–229.
- [3] Friedrichs, K. O., Lax, P. D., 1971. Systems of conservation equations with a convex extension. *Proc. Nat. Acad. Sci.* 68, 1686–1688.
- [4] Godunov, S. K., 1959. Finite difference method for numerical computation of discontinuous solution of the equations of fluid dynamics. *Mat. Sb.* 47, 271.
- [5] Kurganov, A., Levy, D., 2000. A Third-Order Semidiscrete Central Scheme for Conservation Laws and Convection-Diffusion Equations. *SIAM J. Sci. Comput.* 22, 1461–1488.

- [6] Kurganov, A., Noelle, S., Petrova, G., 2001. Semidiscrete Central-Upwind Schemes for Hyperbolic Conservation Laws and Hamilton–Jacobi Equations. *SIAM J. Sci. Comput.* 23 (3), 707–740.
- [7] Kurganov, A., Tadmor, E., 2000. New high resolution central schemes for nonlinear conservation laws and convection-diffusion equations. *JCP* 160, 241–282.
- [8] Levy, D., Puppo, G., Russo, G., May 1999. Central WENO schemes for hyperbolic systems of conservation laws. *Math. Model. Numer. Anal.* 33, 547–571.
- [9] Nessyahu, H., Tadmor, E., 1990. Non-oscillatory central differencing for hyperbolic conservation laws. *J. Comp. Phys.* 87, 408–463.
- [10] Sod, G., 1978. A survey of several finite difference methods for systems of nonlinear hyperbolic conservation laws. *J. Comput. Phys.* 27, 1–31.
- [11] Staniforth, A., Côté, J., 1991. Semi-Lagrangian Integration Schemes for Atmospheric Models – A Review. *Monthly Weather Review* 119, 2206–2223.
- [12] Toro, E. F., 1997. *Riemann Solvers and Numerical Methods for Fluid Dynamics*. Springer-Verlag.
- [13] Vestuto, J. G., Ostriker, E. C., Stone, J. M., Jun. 2003. Spectral Properties of Compressible Magnetohydrodynamic Turbulence from Numerical Simulations. *ApJ* 590, 858–873.